Macroscopic modeling and computation of radiation for a 2m diameter pool fire

By J.F. Ripoll

1. Motivation and objectives

In large pool fires, radiation is the predominant mode of heat transfer (Cox 1995; Tieszen 2001), and its computation is usually time consuming. The use of macroscopic moment models (Modest 2003; Siegel & Howell 2001), which have a lower cost than directly solving the radiative transfer equation (RTE), is thus very attractive. In this paper, the M_1 radiation model, sometimes referred to as *Maximum entropy closure* see (Minerbo 1978; Levermore 1984; Fort 1997; Brunner & Holloway 2001), is chosen to model the radiation field generated by a synthetic fire (Brown & Blanchat 2003).

The first goal of this work is to show the ability of the M_1 model to solve a real fire case occuring in a complex geometry. The fire considered here occurs in the FLAME facility of Sandia Albuquerque, and the particular and complex geometry of this facility will be taken into account. A discussion of the radiative characteristics of the fire will be given to show the coherence of the modeling.

Average opacities, also called effective mean absorption coefficients, are of outstanding importance for radiation modeling. They allow one to take into account, at a macroscopic level, the frequency dependence of the spectral opacity. For fires this spectral coefficient is mainly determined from the soot volume fraction and is linear in frequency. As a result, the mean absorption coefficients are different from the Planck mean absorption coefficient, which constitutes their usual approximation. In this paper, new effective mean absorption coefficients, derived in (Ripoll *et al.* 2001), are used to model the opacity field.

The opacity field is obtained from a computation using the Sandia Vulcan code and accounts for both gas and soot radiation. From this, a global coefficient representative of a mixture of soot and gas is derived and used in the computation of the emission and absorption coefficients.

The first part of this article is a description of the M_1 model, the mean absorption coefficients used therein, and the numerical scheme used for its solution. The second part is devoted to the validation of the M_1 results. In the particular case of two concentric black cold spheres cooling a hot, emitting gas, the solution obtained by the M_1 model is compared to the analytic solution. In the third part, results of the computation of the synthetic fire are given and discussed.

2. Radiative transfer equations

2.1. *The* $\mathbf{M_1}$ *radiative model*

The M_1, or Maximum entropy closure, radiative model (Minerbo 1978; Levermore 1984; Fort 1997; Brunner & Holloway 2001) describes the evolution of the radiative energy E_R

and the radiative flux $\vec{F}_R$ of a non-scattering medium at temperature T.

$$\partial_t E_R + \vec{\nabla} \cdot \vec{F}_R = c\big[\sigma a T^4 - \sigma E_R\big] \tag{2.1a}$$

$$\frac{1}{c}\partial_t \vec{F}_R + c\ \vec{\nabla} \cdot \left(\vec{\vec{D}}_R\ E_R\right) = -\sigma\ \vec{F}_R \tag{2.1b}$$

where c is the speed of light and σ the opacity. The radiative flux has three components in $\mathbb{R}^3$, $\vec{F}_R = (F_R^x,\ F_R^y,\ F_R^z)^T$. The Eddington tensor $\vec{\vec{D}}_R$ is computed from the Eddington factor χ and the anisotropic factor $\vec{f} = (f_x,\ f_y,\ f_z)^T = \vec{F}_R/(cE_R)$:

$$\vec{\vec{D}}_R = \frac{\vec{\vec{P}}_R}{E_R} = \frac{1-\chi}{2}\ \vec{\vec{Id}} + \frac{3\chi - 1}{2}\ \vec{n} \otimes \vec{n} \quad \text{with } \vec{n} = \frac{\vec{f}}{\|f\|} \tag{2.2}$$

where $\vec{\vec{Id}}$ denotes the identity matrix, $\vec{\vec{P}}_R$ is the radiative pressure, and $\otimes$ stands for the dyadic product. The Eddington factor $\chi(\vec{f})$ is a function of the Euclidian norm of $\vec{f}$, $\|f\|$†

$$\chi(\vec{f}) = \frac{3 + 4\|f\|^2}{5 + 2\sqrt{4 - 3\|f\|^2}}. \tag{2.3}$$

The radiative temperature is defined from the radiative energy by

$$T_R = \left(\frac{E_R}{a}\right)^{\frac{1}{4}} \quad \text{with} \quad a = \frac{8}{15}\frac{\pi^5 k^4}{h^3 c^3} \tag{2.4}$$

where k is the Boltzmann constant and h the Planck constant.

2.2. *Computation of mean absorption coefficients*

When the spectral coefficients can be written as polynomial functions of the frequency, it is possible to derive closed formulas for the mean absorption coefficients using the following pseudo-intensity I^* (Ripoll *et al.* 2001):

$$I^* = I(\nu, T^*(\vec{\Omega})) = \frac{2h\nu^3}{c^2}\left[\exp\left(\frac{h\nu}{kT^*(\vec{\Omega})}\right) - 1\right]^{-1} \tag{2.5}$$

where h is the Planck constant, k the Boltzmann constant, ν the frequency, $\vec{\Omega}$ the direction of propagation, and $T^*(\vec{\Omega}) = T/(B(1 - \vec{A}\cdot\vec{\Omega}))$ with $\vec{A}$ and B defined by

$$\vec{A} = \frac{2 - \sqrt{4 - 3\|f\|^2}}{\|f\|^2}\vec{f}, \tag{2.6}$$

$$B = \frac{T}{T_R}\left[\frac{3 + \|A\|^2}{3(1 - \|A\|^2)^3}\right]^{\frac{1}{4}} \tag{2.7}$$

This pseudo-intensity has a Planckian form and maximizes the radiative entropy (or minimizes the mathematical entropy) under the constraint of the reconstruction of the two radiative moments (Minerbo 1978; Fort 1997; Brunner & Holloway 2001). $\vec{A}$ and B are given by this constraint.

When the spectral absorption coefficient is frequency dependent, i.e. when the medium is not gray, this intensity can also be used to define the associated effective absorption coefficients σ_E and σ_F, which are given below.

† $\|g\|$ denotes the Euclidian norm of a vector $\vec{g}$.

For sooty flames, such that the size of the soot particles is much smaller than the mean free path (Rayleigh approximation), the spectral absorption coefficient is linear in frequency, becoming simply $\sigma(\nu) = C_1\nu$, where C_1 depends on the soot volume fraction C_s and is defined in (Smith & Shaddix 1996) by

$$C_1 = \frac{1}{c}\frac{36\pi n\, p\, C_s}{(n^2 - p^2 + 2)^2 + 4n^2p^2},$$

where the values $n \simeq 1.57$ and $p = 0.56$ of (Smith & Shaddix 1996) are used. Hence C_1 is a linear function of the soot volume fraction: $C_1 = 8.33 \times 10^{-9}\, C_s$.

The well-known Planck mean absorption coefficient, σ_P, is given by

$$\sigma_P(T) = \frac{\langle \sigma(\nu)\mathcal{B}(\nu, T)\rangle_{\nu,\Omega}}{\langle \mathcal{B}(\nu, T)\rangle_{\nu,\Omega}} \tag{2.8}$$

where $\mathcal{B}$ is the Planck function and $\langle\mathcal{B}\rangle_{\nu,\Omega}$ denotes the integration of $\mathcal{B}$ over frequency ν and direction Ω. The effective mean absorption coefficients, σ_E and σ_F, are defined and modeled by

$$\sigma_E(t, \mathbf{r}) = \frac{\langle \sigma(\nu) I(t, \mathbf{r}, \mathbf{\Omega}, \nu)\rangle_{\nu,\mathbf{\Omega}}}{\langle I(t, \mathbf{r}, \mathbf{\Omega}, \nu)\rangle_{\nu,\mathbf{\Omega}}} \simeq \frac{\langle \sigma(\nu) I^*(t, \mathbf{r}, \mathbf{\Omega}, \nu)\rangle_{\nu,\mathbf{\Omega}}}{\langle I^*(t, \mathbf{r}, \mathbf{\Omega}, \nu)\rangle_{\nu,\mathbf{\Omega}}} \tag{2.9}$$

$$\sigma_F(t, \mathbf{r}) = \frac{\langle \sigma(\nu)\mathbf{\Omega} I(t, \mathbf{r}, \mathbf{\Omega}, \nu)\rangle_{\nu,\mathbf{\Omega}}}{\langle \mathbf{\Omega} I(t, \mathbf{r}, \mathbf{\Omega}, \nu)\rangle_{\nu,\mathbf{\Omega}}} \simeq \frac{\langle \sigma(\nu)\mathbf{\Omega} I^*(t, \mathbf{r}, \mathbf{\Omega}, \nu)\rangle_{\nu,\mathbf{\Omega}}}{\langle \mathbf{\Omega} I^*(t, \mathbf{r}, \mathbf{\Omega}, \nu)\rangle_{\nu,\mathbf{\Omega}}} \tag{2.10}$$

and are functions of time t and position r. These integrals are computed in (Ripoll *et al.* 2001) and are given by:

$$\sigma_P = 360\; C_1 \frac{k\zeta_5}{\pi^4 h} T = C_P\, T \quad \text{with} \quad C_P = 360\frac{k\zeta_5}{\pi^4 h} C_1 \tag{2.11}$$

$$\sigma_E = 1080 C_1\; \frac{k\zeta_5 T(1 + \|A\|^2)}{h\pi^4 B(3 + \|A\|^2)(1 - \|A\|^2)} \;=\; 3\sigma_P \frac{1 + \|A\|^2}{B(3 + \|A\|^2)(1 - \|A\|^2)}, \tag{2.12}$$

$$\sigma_F = 90 C_1 \frac{k\zeta_5 T(5 + \|A\|^2)}{h\pi^4 B(1 - \|A\|^2)} = \frac{\sigma_P}{4}\frac{5 + \|A\|^2}{B(1 - \|A\|^2)}. \tag{2.13}$$

Using (2.6) and (2.7), the coefficients become

$$\sigma_E = C_P\, G_E(f)\, T_R \quad \text{and} \quad \sigma_F = C_P\, G_F(f)\, T_R \tag{2.14}$$

with

$$G_E(f) = \frac{3}{4}\frac{\left(-1 + \sqrt{4 - 3\|f\|^2}\right)^{1/4}\left(\|f\|^2 - 4 + 2\sqrt{4 - 3\|f\|^2}\right)\|f\|}{\sqrt{\|f\|^2 - 2 + \sqrt{4 - 3\|f\|^2}}\left(-2 + \sqrt{4 - 3\|f\|^2}\right)} \tag{2.15}$$

$$G_F(f) = \frac{1}{4}\frac{\left(-1 + \sqrt{4 - 3\|f\|^2}\right)^{1/4}\left(\|f\|^2 + 4 - 2\sqrt{4 - 3\|f\|^2}\right)}{\sqrt{\|f\|^2 - 2 + \sqrt{4 - 3\|f\|^2}}\|f\|}. \tag{2.16}$$

The M_1 radiative model with mean coefficients becomes

$$\partial_t E_R + \vec{\nabla}\cdot\vec{F}_R = c\left[\sigma_P a T^4 - \sigma_E E_R\right] \tag{2.17a}$$

$$\frac{1}{c}\partial_t \vec{F}_R + c\;\vec{\nabla}\cdot\left(\vec{\vec{D}}_R\; E_R\right) = -\sigma_F\;\vec{F}_R \tag{2.17b}$$

2.3. *Numerical Schemes*

The M_1 model with mean coefficients can be reformulated in a conservative form as follows (Ripoll *et al.* 2002):

$$\partial_t U_R + \nabla_x\, F(U_R) + \nabla_y\, G(U_R) + \nabla_z\, H(U_R) = S_R(U_R, T) \tag{2.18}$$

where

$$U_R = \left(E_R,\ \frac{1}{c}\, F_R^x,\ \frac{1}{c}\, F_R^y,\ \frac{1}{c}\, F_R^z \right) \tag{2.19}$$

$$F(U_R) = (\ F_R^x,\ cD_R^{xx} E_R,\ cD_R^{xy} E_R,\ cD_R^{xz} E_R\ ) \tag{2.20}$$

$$G(U_R) = (\ F_R^y,\ cD_R^{yx} E_R,\ cD_R^{yy} E_R,\ cD_R^{yz} E_R)\,, \tag{2.21}$$

$$H(U_R) = (\ F_R^z,\ cD_R^{zx} E_R,\ cD_R^{zy} E_R,\ cD_R^{zz} E_R)\,, \tag{2.22}$$

$$S_R(U_R, T) = \left(\ c\left(a\sigma_P T^4 - \sigma_E E_R\right),\ -\sigma_F F_R^x,\ -\sigma_F F_R^y,\ -\sigma_F F_R^z\ \right). \tag{2.23}$$

Thus, given a computational field covered with a mesh of control volumes, the partial differential equations can be integrated on these polyhedra. Using Green's formula, this system is discretized in time by an explicit scheme.

$$\frac{U_{R\,i,j,k}^{n+1} - U_{R\,i,j,k}^{n}}{\Delta t} + \frac{\mathcal{F}_{i+1/2,j,k}^{n} - \mathcal{F}_{i-1/2,j,k}^{n}}{\Delta x} \tag{2.24}$$

$$+\frac{\mathcal{G}_{i,j+1/2,k}^{n} - \mathcal{G}_{i,j-1/2,k}^{n}}{\Delta y} + \frac{\mathcal{H}_{i,j,k+1/2}^{n} - \mathcal{H}_{i,j,k-1/2}^{n}}{\Delta z} = S_R(U_{R\,i,j,k}^{n}). \tag{2.25}$$

In order to compute the convective terms, an upwind flux-limited scheme, the HLLE scheme (Hirsch 1990), using Roe's approximate Riemann solver, is used. This scheme applied to the M_1 model approximates the divergence as follows:

$$\begin{aligned}\frac{\mathcal{F}_{i+1/2,j,k}^{n+1} - \mathcal{F}_{i-1/2,j,k}^{n+1}}{\Delta x} = {} & \frac{1}{2\ \Delta x}\left(F_{i+1,j,k}^{n+1} + F_{i,j,k}^{n+1} - c\ \left(U_{R\,i+1,j,k}^{n+1} - U_{R\,i,j,k}^{n+1}\right)\right) \\ & - \frac{1}{2\ \Delta x}\left(F_{i,j,k}^{n+1} + F_{i-1,j,k}^{n+1} - c\ \left(U_{R\,i,j,k}^{n+1} - U_{R\,i-1,j,k}^{n+1}\right)\right)\end{aligned} \tag{2.26}$$

$\mathcal{G}$ and $\mathcal{H}$ are obtained similarly to $\mathcal{F}$ by permutation of i, j, and k. A second order correction which is needed to obtain better accuracy is given in (Ripoll *et al.* 2001).

3. Numerical Validation

This section is devoted to the numerical validation of the M_1 model and of the solver used.

The geometry for this test is the annular region between two concentric spheres. The inner sphere has a radius $R_i = 1.0$ and the outer sphere has radius $R_o = 1.6$. Both spheres have unit transmissivity (zero emissivity) and are exposed to cold black surroundings $I_i = I_o = 0$. The scattering coefficient within the annulus is zero while the absorption coefficient and retardation factor are set to unity. The annulus also has a uniform heat generation rate of $Q = 4\pi$.

With an uncertainty of 0.0005%, the steady state radiative energy is given in (Burns

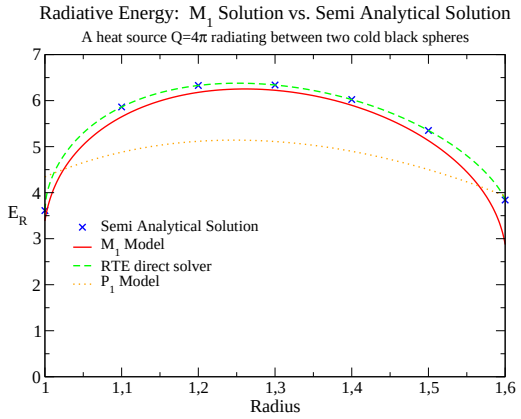

FIGURE 1. Hot gaz radiating between 2 concentric Spheres

2003) as

r	$E_R(r)$	r	$E_R(r)$	r	$E_R(r)$	r	$E_R(r)$
1.0	3.6108	1.2	6.3288	1.4	6.0233	1.6	3.8398
1.1	5.8619	1.3	6.3390	1.5	5.3508		

(3.1)

For the M_1 solver, a domain of 1000 nodes is used to obtain mesh convergence. The steady state solution is converged in time, and the final residue is 10^{-15}.

The solution found by the M_1 solver is in very good agreement with the semi-analytical values and with the solution given by a RTE solver, see Fig. 1. It may also be seen that the M_1 closure constitutes an improvement, compared to a simple closure like P_1, which in this case gives an inaccurate solution. The non-symmetry of the solution and the position of the maximum value, at $r = 1.2$ for the RTE solver and at $r = 1.25$ for M_1, indicates that the three dimensional geometry is well computed. These results demonstrate the accuracy of the method and its solver.

4. Computation of radiation for a pool fire

The domain of computation, describing a quarter of the geometry of the FLAME facility at Sandia Albuquerque, is shown in Fig. 2(left) (Brown & Blanchat 2003). The domain is three dimensional, but can roughly be considered axisymmetric due to the circular bowl containing the fuel and the circular facility for the entering air. All results plotted are in the plane $x = 0.05$, but the computations are done in 3D. The synthetic fire has been computed by A. Brown (Brown & Blanchat 2003) of Sandia Albuquerque. The mesh used for the computation is $31 \times 31 \times 93$. The wall and the bowl are simulated by a very large opacity, $1000\,m^{-1}$, where radiation cannot propagate. The domain is hence considered completely open, and the opacity σ, playing the role of walls, will regulate the radiation field. It must be noticed here that the exact position of the bowl, where the fuel burns, is spread out vertically over two cells, centered at $z = -0.05$ and $z = -0.15$. The first computational cells adjacent to it are $z \in [0., 0.1]$ (white zone), centered at $z = 0.05$.

In Fig. 2(right), the profile of the temperature of the synthetic fire is given. Four zones

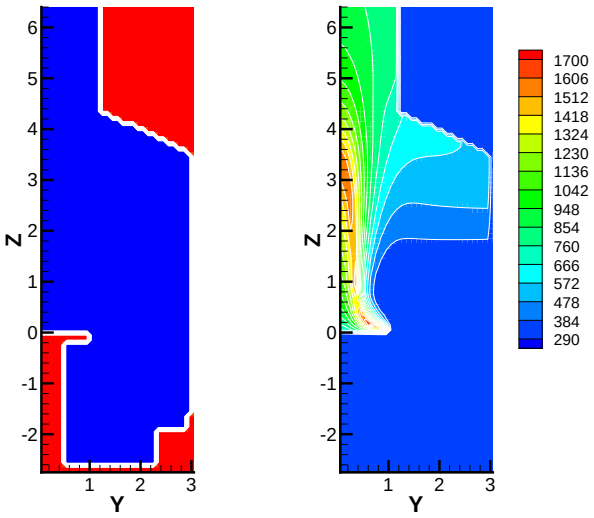

FIGURE 2. 2D cut of the computationnal domain (left); T (right)

can be seen: (1) the flame zone, delimited by the flame front where the temperature is higher, (2) the hot gas region, flowing in the chimney, (3) a moderately high temperature region on the right of the fire (between $400K$ and $700K$), where the opacity is small but not zero, generated by gas trapped by the too small size of the chimney, and (4) a region of quasi-ambient-temperature situated below the bowl. It is assumed that the absorption coefficient σ_s, provided by Sandia, has been determined from a Planck absorption coefficient in which a mixture of soot and gas is considered to radiate with the same optical properties as soot. This last assumption constitutes the main approximation since gaseous flame mixtures are, unlike soot, not gray media. This approximation allows us to determine the volume fraction Y_m of the mixture soot+gas as follows:

$$\sigma_s \simeq \sigma_P(Y_m, T) = C_m Y_m T \simeq C_s Y_m T \tag{4.1}$$

Then $Y_m = \sigma_s/(C_s T)$ gives the mixture fraction of our mixture and is plotted in Fig. 3.

The opacity of the fire is now considered as given from this mixture, and the three mean coefficients $\sigma_P(Y_m, T)$, $\sigma_E(Y_m, T_r, \|f\|)$, and $\sigma_F(Y_m, T_r, \|f\|)$ are used in this computation. These coefficients are plotted in Fig. 4-6. For each of these three figures, the high opacity zone in the flame is shown on the left: the maximal value reaches $10\,m^{-1}$ (zones higher than 10 are red and must be disregarded). The low opacity region, between $1\,m^{-1}$ and $0.1\,m^{-1}$, present close to the fire and in the chimney, is plotted on the right (here zones higher than 1 are red and must be disregarded). The steady state profile of both radiative temperature and energy computed with M_1 are given in Fig. 7. An important remark can immediately be given: the model does not propagate radiation below the bowl, as can be the case with other models, like P_1. The flame zone of the fire admits a high radiative temperature, but lower than the gas temperature, signifying a strong emission in this region. Furthermore, the moderately high temperature region absorbs a small quantity of radiation. The three components of the flux are plotted in Fig. 8. On the left, it can be checked that the x-component of the flux is very low compared to the others, signifying that the profile can be considered as nearly cylindrically symmetric.

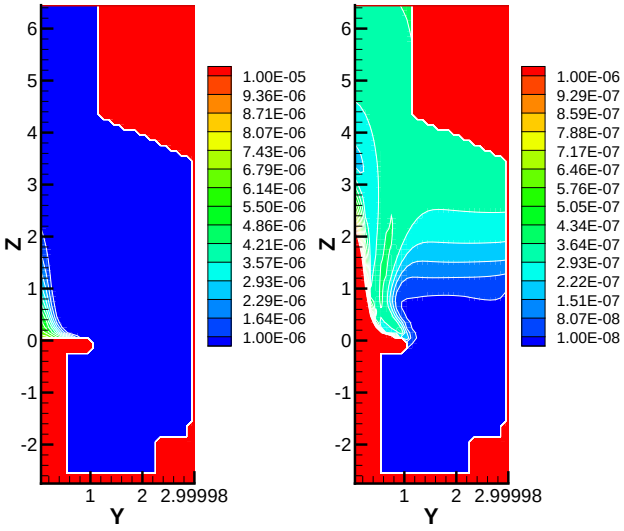

FIGURE 3. Y_m, high volume fraction regions (left), Y_m, low volume fraction opacity regions (right)

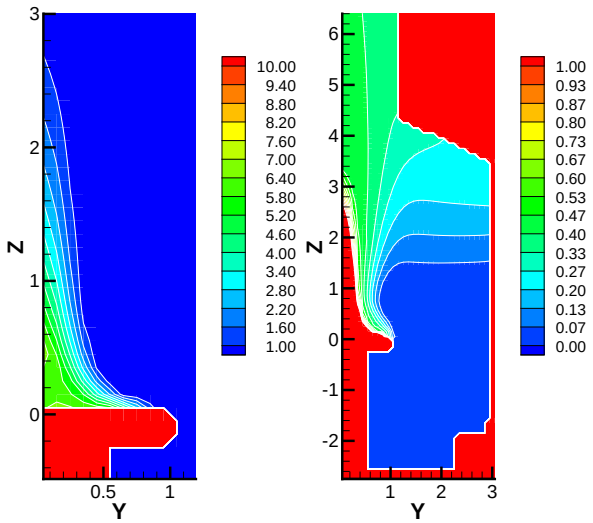

FIGURE 4. σ_P, high opacity regions (left) σ_P, low opacity regions (right)

Moreover the symmetry around to the z-axis can be checked. In Fig. 8(center)-(right), very close to the bowl, a region of negative fluxes can be seen, indicating that the bowl is heated by radiation. Radiation propagates clearly in the direction of the chimney and in the direction of the right wall. Two high temperature zones, one very close to the bowl and the other at $3\,m$ high, emit strongly in both chimney and wall directions, see Fig. 8(right).

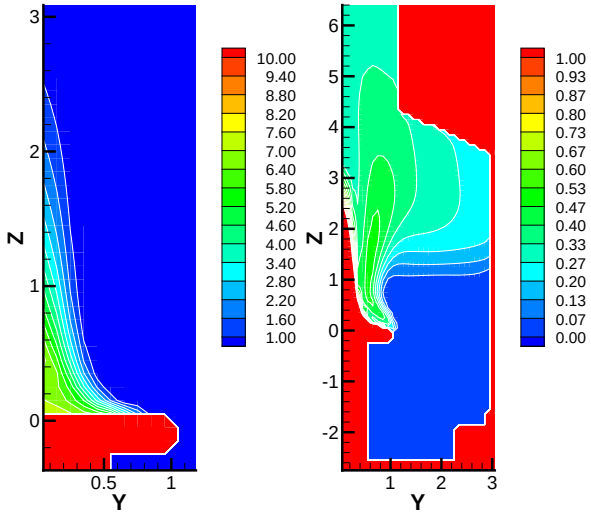

FIGURE 5. σ_E, high opacity regions (left) σ_E, low opacity regions (right)

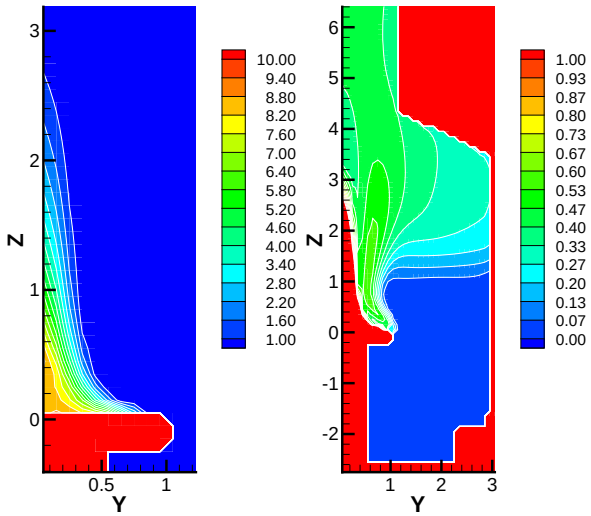

FIGURE 6. σ_F, high opacity regions (left) σ_F, low opacity regions (right)

In Fig. 9(left), the flux vector $\vec{V} = (F_R^y, F_R^z)$ is plotted. The three directions of propagation mentioned before are confirmed: toward the chimney, the wall, and the bowl. An important remark is that radiation does not propagate below the bowl in a pathological way, as we would find using some diffusion methods. In this region, where the opacity is almost zero, it can be seen that no dominant radiation occurs. The anisotropic factor in Fig. 9(center) indicates an isotropic region, central to the fire, where, due to symmetry around the z-axis, the fluxes are very small or zero. At one meter from the center of

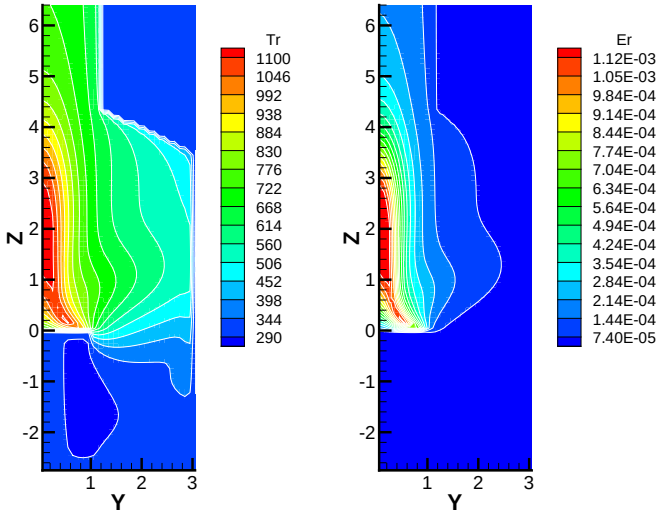

FIGURE 7. T_R (left), E_R (right)

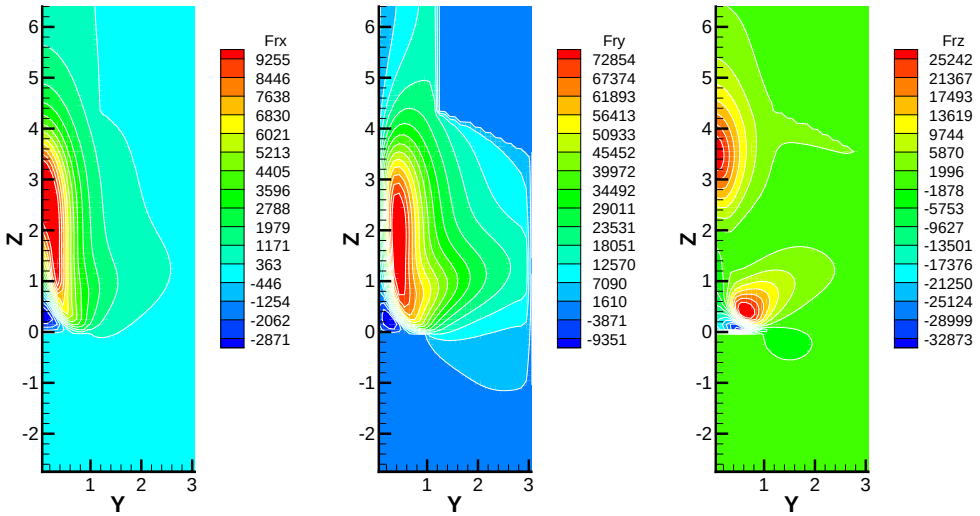

FIGURE 8. F_R^x (right); F_R^y (center); F_R^z (left)

the fire, radiation becomes anisotropic and, from there, isotropic models, like P_1, should not be used. The most anisotropic region is situated far from the fire, close to the wall, almost below the bowl, and "*sees*" the fire through a small window. The small opacity and angle of view explain this anisotropy region where $\|f\|$ reaches its maximal value of 0.94.

In Fig. 10, the radiative net heat flux, i.e. $c(\sigma_P a T^4 - \sigma_E E_R)$, which is the coupling term intervening in the energy conservation equation of Navier-Stokes (modulo the sign)

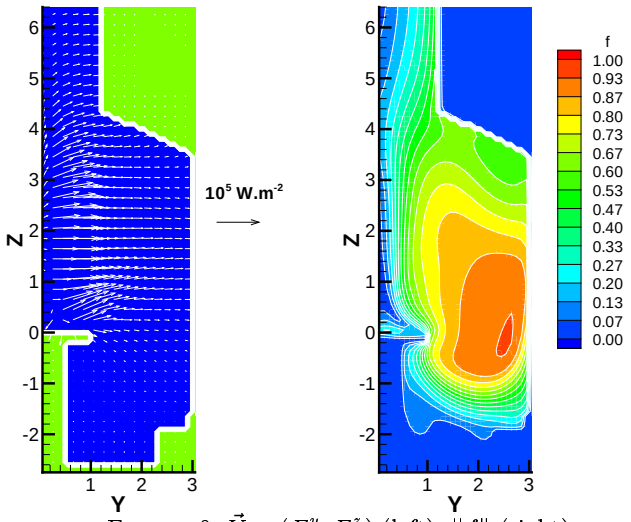

FIGURE 9. $\vec{V} = (F_R^y, F_R^z)$ (left); $||f||$ (right)

is plotted. Three ranges of scale have been chosen in order to differentiate the absorption zones from the emission ones. In the first figure, Fig. 10(left), the blue zone must be disregarded, as must be the red one in the next figure, and both blue and red ones in the third figure. In Fig. 10(left), the non-blue region of the flame zone indicates a strong region of emission. In Fig. 10(center), exactly in the first cells adjacent to the bowl, a strong absorption region can be seen. This indicates that the bowl is heated by the fire in a strong way, where we know it participates in an important way in the vaporization of the fuel. The vaporization process conditions the whole fire flow, and it is hence particularly important to predict it accurately. An accurate computation of the absorption of radiation is thus very important in this region. Moreover, a few centimeters higher, the hot gas in the flame cone region, not yet reacting, also absorbs heat from the flame zone. Finally it can be noticed that the wall of the chimney absorbs some heat as well. In Fig. 10(right) are plotted the regions where a low but non-negligible absorption occurs. The fire is bounded to the right by an absorption zone, which confines the heat. The right wall absorbs some heat as well. Finally, below the bowl, neither absorption or emission occurs.

5. Conclusion

A model of radiation using a moment method has been proposed for fires. The models for the transport of radiation, for the computation of the opacities, and their discretizations have been presented. A pool fire occuring in a complex geometry has been computed by this model. The results are found to be coherent and consistent. This model thus seems to constitute a good alternative to the solving of radiation by direct RTE methods, which are more costly. This work constitutes the preliminary results of a much bigger project involving the collaboration of NASA Ames, Sandia Albuquerque, and Ecole des Mines d'Albi. In this project, the radiation of a fire, which is comparable to the one studied

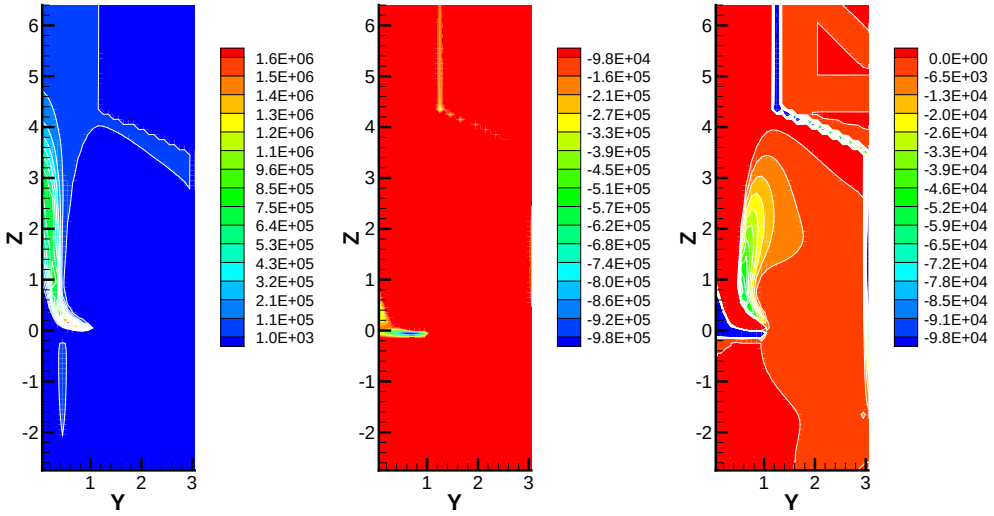

FIGURE 10. Positive net heat flux (left); Strong negative net heat flux (center); Low negative net heat flux (right)

here, will be solved by several methods, including this one, and compared (Jensen *et al.* 2004).

Acknowledgments

The author would like to thank Dr. Alexander Brown of Sandia National Laboratories who provided the temperature and opacity profiles of the fire which has been used in this work. Particular thanks are addressed to Dr. Kirk Jensen and Dr. Sheldon Tieszen of Sandia National Laboratories for their extensive technical discussions and support.

REFERENCES

BROWN, A.L., & BLANCHAT, T.K. 2003 A validation quality heat flux dataset for large pool fires. *2003 ASME Summer Heat Tansfer Conference, Las Vegas HT2003-40249.*

BRUNNER, T. A., HOLLOWAY, J. P. 2003 One-dimensional Riemann solvers and the maximum entropy closure. *Jour. Quant. Spectrosc. Radiat. Transfer*, **69**, 543-566.

BURNS, S. P. 2003 SYRINX User manual. Preprint in progress, Sandia National Laboratories, Albuquerque.

COX, G. 1995 Combustion fundamentals of fires. Academic Press.

FORT, J. 1997 Information-theoretical approach to radiative transfer. *Phys. A.*, **243**, 275-303.

HIRSCH, C. 1990 Numerical Computation of Internal and External Flows. Nb. 1-2. *Wiley Interscience Publication.*

JENSEN, K. A., RIPOLL, J.-F., WRAY, A. A., JOSEPH, D., EL-HAFI, M. 2004 Radiative transfer modeling of a large pool fire by discrete ordinates, discrete transfer, ray

tracing, Monte Carlo, and moment methods. *Proceedings of the center for turbulence research summer programm*, in preparation.

LEVERMORE, D. 1984 Relating Eddington factors to flux limiters. *Jour. of Quant. Spectrosc. & Radiat. Transfer*, **32(2)**, 149-160.

MINERBO, G. N. 1978 Maximum entropy eddington factors. *J. Quant. Spectrosc. Radiat. Transfer* **20**, 541–545.

MODEST, M.F. 2003 Radiative heat transfer. 3rd ed., McGraw-Hill.

RIPOLL, J.-F., DUBROCA, B. & DUFFA, G. 2001 Modelling radiative mean absorption coefficients. *Comb. Th. and Mod.* **5** (3), 261–275.

RIPOLL, J.-F., DUBROCA, B., AUDIT, E. 2002 A factored operator method for solving coupled radiation-hydrodynamics models. *Trans. Theory and Stat. Phys.*, **31**(4-6), 531-557.

SIEGEL, R. C. & HOWELL, J. R. 2001 *Thermal radiation heat transfer*. 4^{th} Ed., Taylor and Francis.

SYMTH, K. C., SHADDIX C. R. 1996 The Elusive history of $\tilde{m} = 1.57 - 0.56i$ for the refractive index of soot. *Comb. and Flame*, **107**, 314-320.

TIESZEN, S. R. 2001 On the fluid mechanics of fires *Annu. Rev. Fluid Mech.*, **33**, 33-67.